Dalton Transactions

PAPER

View Article Online
View Journal | View Issue

Cite this: *Dalton Trans.*, 2019, **48**, 5952

Synthesis, structure, docking and cytotoxic studies of ferrocene–hormone conjugates for hormone-dependent breast cancer application†

José A. Carmona-Negrón,[a] Alberto Santana,[a] Arnold L. Rheingold[b] and Enrique Meléndez *[a]

Received 8th May 2018,
Accepted 21st November 2018

DOI: 10.1039/c8dt01856a

rsc.li/dalton

Previously, ferrocene incorporation into the principal structural component of biologically active molecules resulted in enhanced cytotoxic activity against hormone-dependent MCF-7 and T-47D and hormone-independent MDA-MB-231 breast-cancer cell lines. Here we explore 4 new ferrocene estrogen conjugates at position 16 of the estrogen hormone and compared them to the previously reported ferrocene estrogen conjugate 3-ferrocenyl-estra-1,3,5(10)-triene-17β-ol. The ferrocene conjugate 16-ferrocenylidene-3-hydroxyestra-1,3,5(10)-trien-17-one was synthesized using estrone and ferrocene carboxaldehyde as starting materials in 86% yield. This ferrocene complex was used as the starting material for the synthesis of new ferrocene estrogen conjugates by a short linker group at position 16 of the estrogen hormone. The position and stereochemistry of the linker was verified by its crystal structure. The ferrocene redox behavior, *in vitro* studies on breast-cancer cell lines and docking studies on ERα are presented. The data suggest that the ferrocene conjugates presented, either at position 3 or 16 of the estrogen, could serve as vectors and can be recognized by ERα as a delivery mechanism into the cell. These new ferrocene hormone conjugates showed cytotoxic activity comparable to that of conventional therapeutic drugs such as tamoxifen and cisplatin.

Introduction

Cisplatin and its derivatives have been, for decades, the role models of successful metal-based therapeutic anticancer drugs. Their wide range of application on different cancers, such as testicular, ovarian, breast, brain, lung,[1] among others,[2] demonstrated that cisplatin and its derivatives are one of the most dynamic cancer drugs ever discovered. The particularly powerful antineoplastic activity of cisplatin is due to its non-reversible and covalent crosslinking with the purine bases on DNA, interference with DNA repair mechanisms, DNA damage, and subsequent induction of apoptosis in cancer cells.[3] However, its successful history has been followed by the shadow of its side effects that up until today, is the major limitation.[4] Among the cisplatin side effects, neurotoxicity[5] and nephrotoxicity[6] have been identified as the most severe ones related to its therapeutic treatment, but also, cancer resistance development to this type of therapy has been identified as another limitation.[7] One of the challenging aspects to develop a more robust and efficient platinum-based therapeutic drug for cancer treatment comes from the fact that cisplatin lacks biologically-active ligands that could be recognized by biological markers and receptors which are overexpressed on cancer cells. Thus, this renders the drug without an efficient delivery mechanism before and after reaching the cancer tissue. Additionally, the drug is a target for hydrolytic decomposition in an aqueous environment. Since then, the synthesis of other metal-based compounds has been pursued with antineoplastic activity and less toxic side effects than cisplatin and its derivatives.

In the last thirty five years, ferrocene has been introduced for biological applications due to its antineoplastic properties on Ehrlich ascites tumor.[8] In contrast to cisplatin and its derivatives, ferrocenes exhibit a series of desired physical and chemical properties such as aqueous stability and synthetic chemistry highly homologous to that of benzene. In addition to its aromatic properties, the fact that it exhibits a redox behavior makes ferrocene an excellent candidate for drug

[a]*University of Puerto Rico, Department of Chemistry, PO Box 9019, Mayagüez, PR 00681, Puerto Rico. E-mail: enrique.melendez@upr.edu*
[b]*University of California–San Diego, Department of Chemistry and Biochemistry, Urey Hall 5128, 9500 Gilman Drive, La Jolla, CA 92093-0358, USA*

† Electronic supplementary information (ESI) available. CCDC 1842140–1842145. For ESI and crystallographic data in CIF or other electronic format see DOI: 10.1039/c8dt01856a

development.[9–12] Its anticancer activity is due to the metabolic formation of ferrocenium that induces oxidative damage to DNA due to the formation of radical oxygen species (ROS) into the cell.[13–15] To enhance the cytotoxic activity, ferrocene has been successfully conjugated to molecules that have biological activity.[16,17] In this regard, Jaouen *et al.* explored the incorporation of ferrocene into a hydroxytamoxifen (OH-TAM) frame.[18] The resulting hydroxyferrocifen is one of the most successful ferrocene conjugates with antineoplastic activity against breast cancer.

In 2011 our group reported a series of ferrocene group successfully incorporated into the hydroxyl group on the estrogen C(3) position of estrone and estradiol, and studied their cytotoxic activities on the hormone-dependent MCF-7 breast-cancer cell line.[19] Among them, estradiol derivatives showed high cytotoxic activity. Computational docking studies on a 3-estradiol ferrocenecarboxylate conjugate were performed on the Estrogen Receptor alpha (ERα) Ligand Binding Domain (LBD) demonstrating its capability to dock into the ligand binding pocket (LBP). However, a more detailed evaluation of the ligand binding pocket led us to explore other structural variants that could bind into the ERα-LBD. Based on this analysis, we changed the strategy and evaluated the estrogen C-16 position for the ferrocene–estrogen conjugates that potentially have a similar volume distribution to 3-estradiol ferrocenecarboxylate and potentially may dock into the ERα-LBD. This ferrocene–hormone conjugate displays micromolar cytotoxic activity on the hormone-dependent MCF-7 and T-47D and hormone-independent MDA-MB-231 breast cancer cell lines, which is similar to conventional therapeutic drugs, such as tamoxifen and cisplatin. To determine, unequivocally, the structural features of these complexes and use these data as the cornerstone to understand their structure–activity relationship on hormone-dependent breast cancer cell lines, the ferrocene conjugates have been fully characterized by X-ray crystallography. In addition, computational studies of the interaction of the ferrocene conjugates with the ERα-LBD were performed, suggesting the possibility of docking of these ferrocene–hormone conjugates into the ligand binding pocket and receptor recognition.

Results and discussion

Three main factors were considered to understand the antineoplastic activity of the ferrocene–estrogen conjugates on hormone-dependent and hormone-independent breast-cancer cell lines. First, the position of the ferrocene group in the main skeleton of the estrogen hormone. Second, the effect of ferrocene functionalization on its redox properties and third, the *in-silico* docking analysis of each ferrocene conjugate in the ERα as the main overexpressed protein in hormone-dependent breast cancer cell lines. The X-ray crystallography studies were a key factor for, not only to fully characterize each ferrocene conjugate, but also to understand, at the structural level, some of the intrinsic properties of each conjugate on the previously mentioned areas.

Chemistry

The synthesis of 3-estradiol ferrocenecarboxylate (**1**) by the reaction of ferrocenecarbonylchloride and the estradiol C(3) hydroxyl group was previously reported by our group.[19] However, here we present a more useful and versatile synthetic approach for it (Fig. 1). 3-Estradiol ferrocenecarboxylate was synthesized using estradiol and fluorocarbonylferrocene[20] as starting materials, in dry CH_2Cl_2 and 4-(dimethylamine) pyridine (DMAP) in 85% yield. This yield remarkably contrasts (nearly twice) with the previous synthetic methodology approach that was employed using the highly reactive species ferrocenylcarbonylchloride as a starting material (40–45% yield).

On the other hand, estrogen's D ring substitution on the C(16) position was achieved using estrone and ferrocene carboxaldehyde as starting materials through an aldol condensation to afford 16-ferrocenylidene-3β-hydroxyestra-1,3,5(10)-triene-17-one (**2**) in 86% yield,[21] Fig. 2. From this reaction pathway we isolated only the *E* isomer. The presence of the *Z* isomer was not evident at the time of purification by column chromatography. In addition, the *E* isomer being the most abundant and crystallization being the method of isolation, the small presence of the isomer *Z*, if any, could have been excluded in the nucleation process. One of the possible explanations for obtaining only the *E* isomer is the steric hindrance possibly experienced by the carbonyl group and the Cp hydrogens on the *Z* isomer if both groups are positioned in the same plane.

Product **2** (*E* isomer) was able to be isolated as 2 conformers (**2a** and **2b**) in the solid state, in which the ferrocene's aromatic cyclopentadienyl ring adopts a coplanar conformation with the olefinic group of the α,β-unsaturated system. The two crystal structures of **2** (**2a** and **2b**) were obtained using different crystallization media, benzene and carbon tetra-

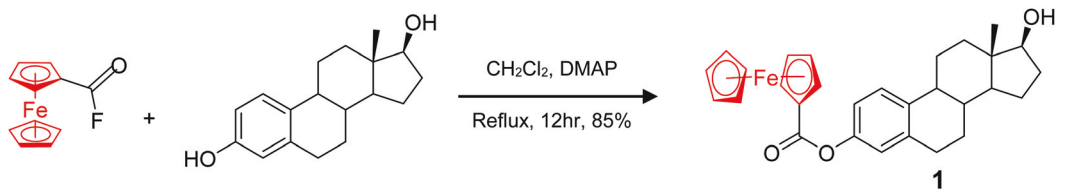

Fig. 1 Synthetic route to target compound **1**.

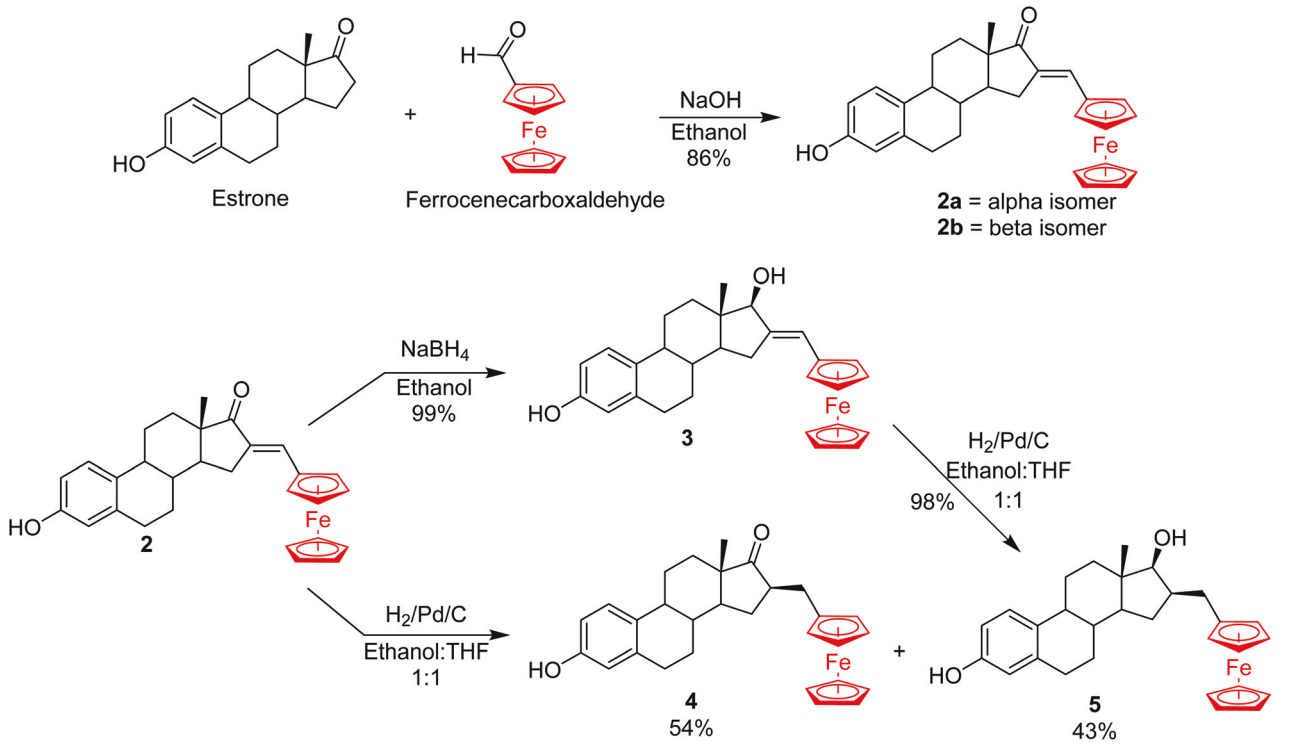

Fig. 2 Schematic representation of the synthetic route to target each of the ferrocene–estrogen conjugates at position 16.

chloride respectively (*vide infra*). However, the NMR data showed the presence of one species, indicating that the two conformers have a low rotational-barrier energy.

For subsequent reactions, ferrocene conjugate **2** was used as the starting material to obtain 16-ferrocenylidene-17β-estra-1,3,5-triene-3,17-diol (**3**), 16-ferrocenemethyl-3β-hydroxyestra-1,3,5(10)-triene-17-one (**4**) and 16-ferrocenemethyl-17β-estra-1,3,5(10)-triene-3,117-diol (**5**). Compounds **4** and **5** were obtained as single diastereomeric products as a consequence of the new stereogenic centers at C(16) and C(17). These two compounds were formed after catalytic hydrogenation: the partial reduction of the olefinic bond led to **4** and the complete reduction of both the carbonyl and double bond of compound **2** led to the formation of **5**. After chromatographic purification, **4** and **5** were isolated in 54% and 43% yield, respectively. The selective reduction of the carbonyl group on **2** can only be achieved using $NaBH_4$ in ethanol, obtaining **3** in 99% yield. Compound **5** can also be obtained from the carbonyl reduction of **4** (same conditions as **3**) in 98% yield.

Crystallography

The solid-state characterization of the new species provided valuable information regarding the stereochemistry and some unexpected geometrical features. The molecular structures of all the ferrocene conjugates were determined by single crystal X-ray diffraction techniques. Table S1† summarizes selected bond distances and angles and Fig. 3 shows the ORTEP diagrams.

3-Estradiol ferrocenecarboxylate (**1**) was previously synthesized but its molecular structure was not published.[19] Its structure confirmed that esterification was achieved on the O(1) phenoxy group, by positioning the ferrocene between the alpha and beta faces of the steroid. The dihedral angle between the phenyl plane and the cyclopentadienyl carboxylate is 86.5°. As previously observed in other steroids, the angle around the carbon substituted with the methyl group, (C(13)), has a substantial contraction (100.1(5)°) from the ideal 108°, although none of the remaining angles in the five-membered ring approaches 108°.

The 16-ferrocenylidene estrone complex is more intriguing with remarkable features since we were able to isolate in the solid state two conformers, alpha (**2a**) and beta (**2b**). **2a** co-crystallizes with a benzene molecule on the unit cell and has hydrogen-bonds between the phenol on one side and the ketonic oxygen of the steroid on the neighboring unit cell. On the other hand, **2b** co-crystallizes with CCl_4 in the unit cell and the packing system shows a similar hydrogen-bond network to **2a** (head to tail) among the hormone moieties, but also a halogen bond between CCl_4 and O(1). The solid state structure of **2a** has the ferrocene positioned on the alpha face of the steroid skeleton with a torsion angle (C(16)–C(19)–C(20)–Fe) of 79.1(3)°. The olefin link to the steroid (C(16)–C(19)) is 1.345(3) Å, typical of a double bond. Although the C(17)═O(2) bond is slightly longer (1.225(3) Å) than the C═O bond in estrone (1.219(2) Å), this bond length together with the olefin link (1.345(3) Å) suggests there is no delocalization between these two functional groups. The dihedral angle C(16)–C(19)–C(20)–

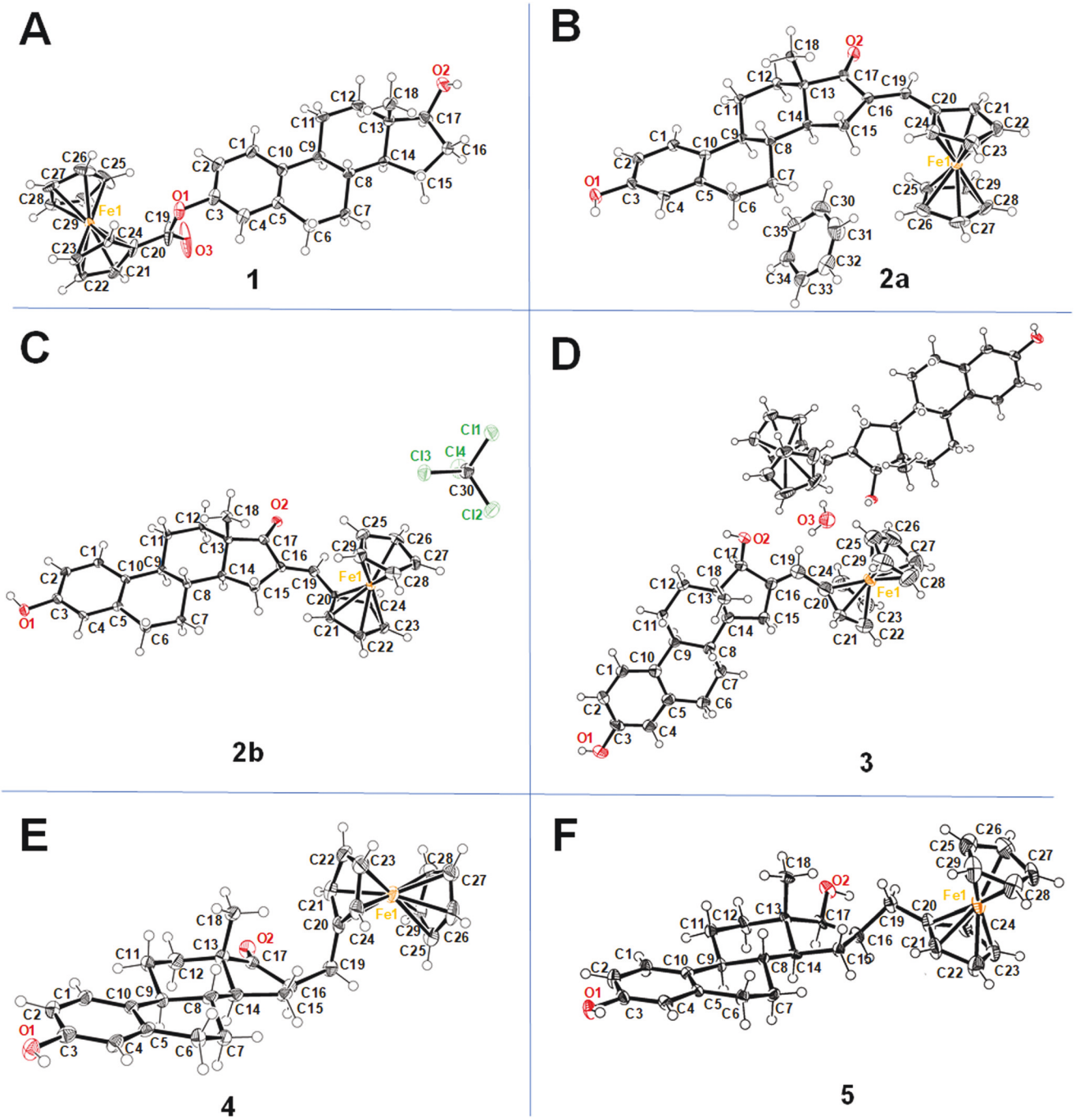

Fig. 3 ORTEP diagrams of 3-estradiol ferrocenecarboxylate (A), 16-ferrocenylidene estrone alpha (B), 16-ferrocenylidene estrone beta (C), 16-ferrocenylidene estradiol (D), 16-ferrocenylmethyl estrone (E), and 16-ferrocenylmethyl estradiol (F). Displacement ellipsoids are drawn at the 50% probability level. ORTEP diagram of **5** showing only one of the six crystallographic molecules in the unit cell for clarity. Numbering of the estrogen principal component of each ferrocene complex is according to the estrogen's nomenclature.

C(21) is 167.72(3)°, which also suggests the olefin is not delocalized with the Cp ring. The angle on the substituted carbon C(13), C(17)–C(13)–C(14), 100.6(2)° shows substantial contraction as typically observed in the five-membered ring of steroids. The structure of **2b** has the ferrocene positioned on the beta face of the steroid with a torsion angle C(16)–C(20)–C(21)–Fe of 253.34(3)°. In an analogous manner to the alpha rotamer, the olefin (C(16)–C(20), 1.341(6) Å) and the carbonyl (C(17)–O(2), 1.236(5) Å) groups are not delocalized. Furthermore, the dihedral angle C(16)–C(19)–C(20)–C(21) is 161.44(7)°, which also suggests the olefin is not delocalized with the Cp ring. Notably, the olefinic carbon in both structures deviates from a typical sp^2 hybridization, with angles of 128.9(2) for **2a** and 128.0(4)° for **2b**, most likely to minimize

steric interactions between the Cp and the steroid cyclopentane ring. It is worth mentioning that all the ferrocene conjugates showed similar contractions on C(13) of the five-membered ring as well as similar structural features, as described above, on the steroid skeleton.

The 16-ferrocenylidene estradiol (**3**) showed two crystallographically independent molecules: one with the ferrocene positioned between alpha and beta faces (Fe(A)), and the second one with the ferrocene on the beta face (Fe(B)). There is one molecule of water in the unit cell that makes a hydrogen network with the hydroxyls of six-membered rings and there are hydrogen bonds between the phenol OH group of one molecule and the C(17)–OH of the next one. The isomer with the ferrocene between alpha and beta faces has a torsion angle (C(16A)–C(19A)–C(20A)–Fe(A)) of 43(1)°, while for the beta isomer (C(16B)–C(19B)–C(20B)–Fe(B)) it is 82.4(9)°. The solid-state structures of **2** and **3** strongly suggest that different conformers may exist in solution but only two are selectively crystallized in the solid state. The 16-ferrocenylmethyl estrone (**4**) structure confirmed the reduction of the double bond at C(16) with a C(16)–C(19) distance of 1.52(1) Å, by positioning the ferrocene in the steroid beta face with a C(16)–C(19)–C(20)–Fe torsion angle of 172.7(5)°.

The solid-state structure of **5** showed six different conformers in the unit cell (Fig. 4), ranging from alpha to beta faces (62.96 to 206.98°). This clearly shows the reduction of the double bond and that the rotational barrier between the different conformational isomers is very low and all possible orientations exist in equilibrium. In **5**, there are two molecules of ethanol per unit cell forming hydrogen-bonds with OH(3) and OH(17) hydroxyl groups. It is evident that the strong intermolecular hydrogen-bond interaction is a key driving force in the packing system on each ferrocene conjugate. In particular **5**, which results in a high Z' packing system, where the overall energetic contribution of the system by the hydrogen-bond network could overcome the unfavorable intramolecular interactions of each of the different conformers found in the crystal structure.[19] However, it's worth mentioning that less than 1% of all the organometallic structures in crystallographic databases[20] are obtained with a Z' value of 6. Fig. S1 and S2† show the crystal structure packing and H-bond assembling formed in the solid state of each ferrocene–estrogen conjugate.

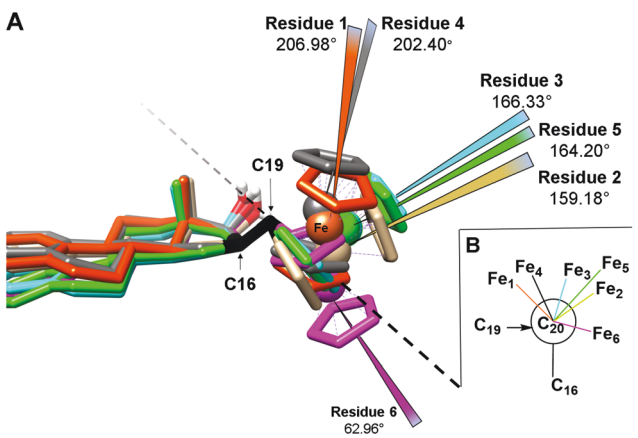

Fig. 4 (A) Superposition on the C(16)–C(19) bond (**black**) of each one of the six-individual residues of complex **5** found in the crystal structure with each one of its dihedral angles around C(16)–C(19)–C(20)–Fe. Hydrogen atoms are omitted for clarity. The dashed line is intended to enhance the visual 3D perspective, and cross through the C19–C20 bond of complex **5** to denote free rotation around it. (B) Newman projection superposition of each of the six-individual residues of complex **5**. Hydrogens of C19 and cyclopentadienyl rings are omitted for clarity.

Electrochemistry

Previous mechanistic studies have established a relationship between the DNA damage capability that exhibit the ferrocene derivatives with their cytotoxic and genotoxic properties.[13–15] The antineoplastic activity of ferrocene is attributed to the facile formation of ferrocenium, which subsequently produces reactive oxygen species (ROS) in the cells, inducing genotoxicity. Given that the conjugates are not soluble in water, the cyclic voltammetry experiments were performed in CH_3CN and compared to the ferrocene/ferrocenium redox couple in acetonitrile, see Table 1. Fig. 5 shows the cyclic voltammograms of ferrocene complexes **2**, **3**, **4**, and **5**. We initially expected to determine the redox behaviors of different ferrocenes according to resonance and inductive effects of each type of functionalization on the Cp ring among the ferrocene conjugates. Complex **2** shows the higher *Epa* due to the strongest electron-withdrawing inductive effect of the

Table 1 Redox potential of ferrocene–estrone conjugates

Ferrocene conjugates	ΔE (mV)	$E_{1/2}$ (mV)
(**1**) 3-estradiol ferrocenecarboxylate	90	711
(**2**) 16-ferrocenylidene-3β-hydroxyestra-1,3,5(10)-triene-17-one	78	565
(**3**) 16-ferrocenylidene-17β-estra-1,3,5-triene-3,17-diol	77	410.5
(**4**) 16-ferrocenemethyl-3β-hydroxyestra-1,3,5(10)-triene-17-one	76	422
(**5**) 16-ferrocenemethyl-17β-estra-1,3,5(10)-triene-3,117-diol	80	389
Fc/Fc^+	84	452

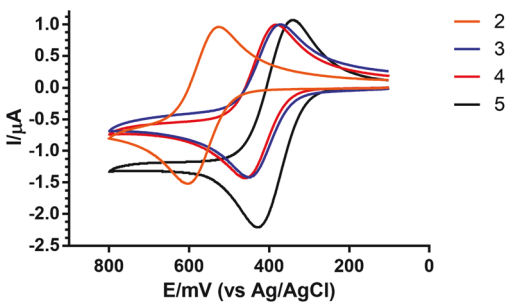

Fig. 5 Cyclic voltammograms of 16-ferrocenylidene estrone (**2**), 16-ferrocenylidene estradiol (**3**), 16-ferrocenylmethyl estrone (**4**), and 16-ferrocenylmethyl estradiol (**5**). The three electrodes used were platinum disk as the working electrode, Ag/AgCl(s) as a reference electrode, and Pt wire as an auxiliary electrode.

enone group, while **4** and **5** show the lowest *Epa*, due to the inductive electron-donation capacity of the methylene group. However, **3** was initially expected to show an *Epa* value between **2** and, **4** and **5**, due to the possibility of the electron-withdrawing inductive effect of the olefinic group, but to a lesser extent than the enone group. It is evident, after analysis of the crystallographic data, that C(16)–C(19) and C(19)–C(20) bond distances of **3** are consistent with the double and single bond distances, respectively, as previously described, where free rotation around C(19)–C(20) is allowed. Therefore, there is no electron delocalization between the Cp ring and the olefinic group. Thus, the ferrocene electrochemical behavior of **3** is similar to **4** and **5** suggesting that there is a minimal influence of the pendant group on the ferrocene redox behavior.

Computational

To understand the cytotoxic activity of the ferrocene–hormone conjugates, and to have a possible mechanistic framework of the role of these conjugates, we performed *in silico* ligand–protein docking with ERα. The scores provided by the AutoDock Vina program (defined by the software as ligand affinity and its predicted affinity energy, in terms of kcal mol^{-1}) were used as parameters to compare the relative binding interaction among the ferrocene–estrogen conjugates and the protein ligand-binding site. The goal of this study was to investigate the potential of estrogens as vectors for ferrocene. Thus, the crystal structure of the estrogen receptor ligand binding domain docked with a europium–estradiol conjugate was selected (pdb:**2YAT**). This structure has an agonist conformation. Typically, ERα antagonists have more volume than agonists, which result in a binding site larger than the one with the agonist conformation. As a result, the docking of these conjugates inside the LBP only suggests the possibility of the selected estrogens to become vectors and be recognized by the receptor. Once inside the LBP, the ferrocene may or may not elicit its cytotoxic effect.

The composition of the estrogen-receptor binding site pocket consists of two subunits separated by a water molecule and the amino acid residues of Glu353 and Arg394. While the major subunit (the one containing the estradiol molecule) has a volume of 233 $Å^3$, the second subunit has a volume of 248 $Å^3$, Fig. 6. The total volume determined using the POVME algorithm was 484.2 $Å^3$. This value is consistent with the volume previously found by Brzozowski *et al.*[20] (450 $Å^3$, pdb:1ERE). Docking studies were performed in two ways: with and without crystallographic water in the ERα-LBD structure, to obtain a more detailed view of the role of water on the ligand–protein binding energy.

The docking studies performed with the water molecule hydrogen-bonded to Glu353 and Arg394 showed that the ferrocene conjugates cannot enter into the estradiol LBP. Therefore, we proceeded to perform the ligand–protein docking without water. To justify the water removal, we calculated the water molecule interaction as well as the ferrocene–LBP interaction. To perform the water docking, we initially removed the water molecule from the crystal structure and performed the docking with the search engine box centered at the same water position in the crystal structure. We performed the same computational protocol used for the ferrocene conjugates by positioning the LBD at the center of the grid and allowing the water molecule to freely move and dock into the LBP. The docked-water calculation result was able to replicate the original position of the water molecule in the crystal structure, showing the characteristic hydrogen-bonding network between Glu353 and Arg394. As a result, docked water shows a predicted binding affinity (BA) of −1.4 kcal mol^{-1}. We employ the same search box to dock the ferrocene molecule, where it shows a BA of −4.2 kcal mol^{-1}. Moreover, when ferrocene is re-docked in the same docking position and residue coordinates of the ferrocene-conjugate **1** (Fig. 6, without water and flexible residues), it shows a BA of −5.7 kcal mol^{-1}. In fact, the docked ferrocene almost superimposes on the ferrocene group of **1**, Fig S3.† Thus, the assumption of removal of water in the ERα-LBP structure is justified. Water interaction is much less than ferrocene–LBP interaction, −1.4 kcal mol^{-1} *vs.* −4.2 kcal mol^{-1}.

The docking studies without water revealed that all conjugates are engulfed in the ERα-LBP. Fig. 7 shows the relative pose and docking score affinity (binding affinity) for each

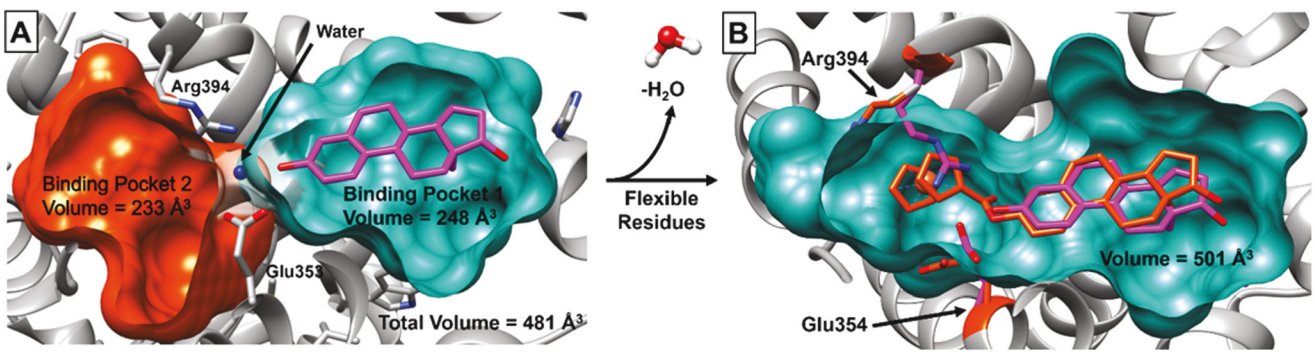

Fig. 6 ERα-LBD cross-section volume contour illustration. (A) Estradiol position (**magenta**) into the ligand binding domain pocket 1 (**turquoise**). The narrow connectivity between pockets 1 and 2 (**orange**) is due to the hydrogen-bond network between Arg394 and Glu354 residues and a water molecule (**blue**). (B) 3-Estradiol ferrocenecarboxylate docking position (**orange**) and the new ERα-LBD volume contour after water removal and residue movements.

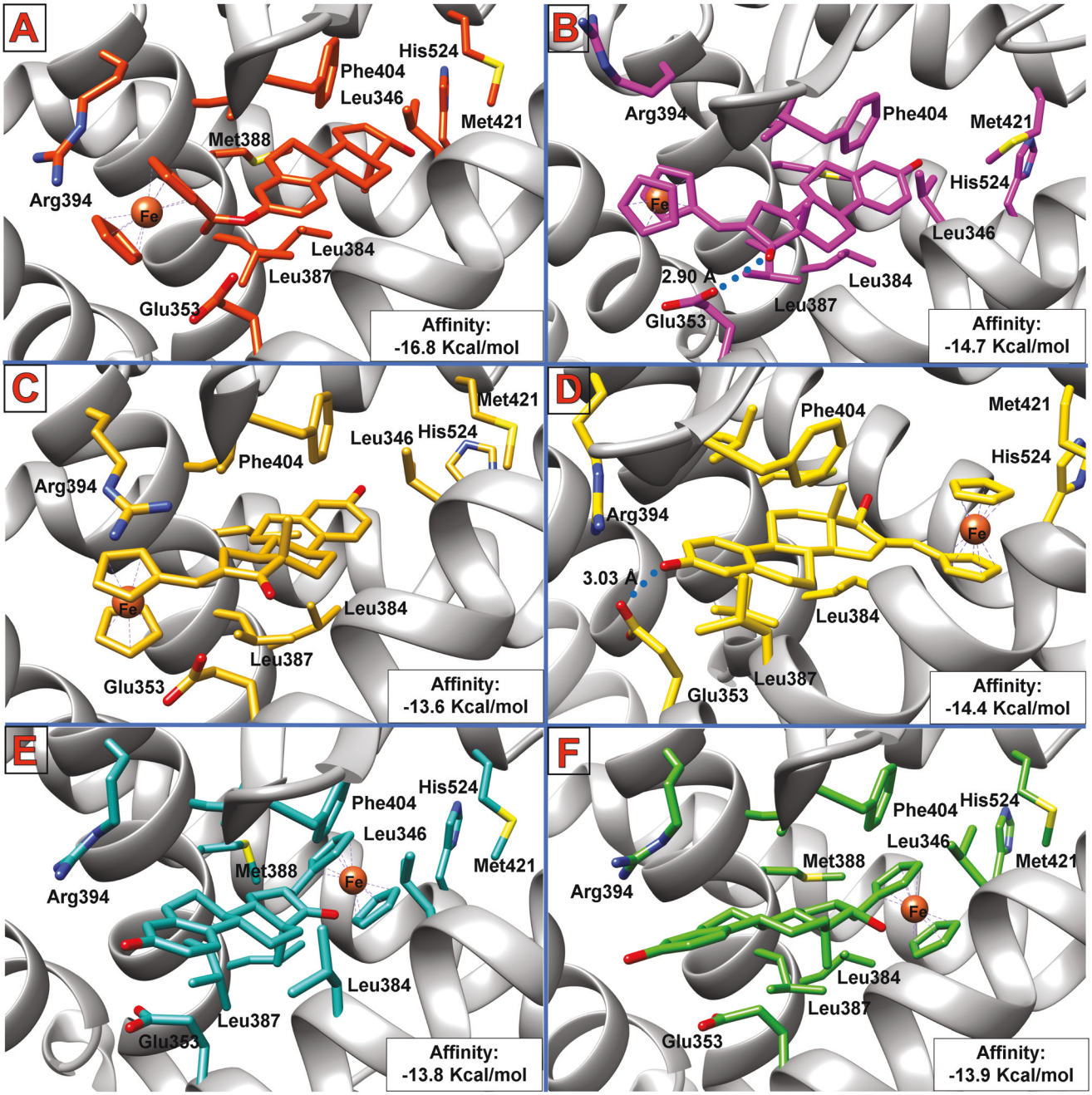

Fig. 7 Docking results of ferrocene conjugates into the ERα-LBD for: 3-estradiol ferrocenecarboxylate, **1** (A). 16-Ferrocenylidene-17β-estra-1,3,5-triene-3,17-diol, **3** (B), 16-ferrocenylidene-3β-hydroxyestraestra-1,3,5(10)-triene-17-one, **2a** and **2b** (C and D), 16-ferrocenemethyl-3β-hydroxyestra-1,3,5(10)-triene-17-one, **4** (D), and 16-ferrocenemethyl-17β-estra-1,3,5(10)-triene-3,117-diol, **5** (E).

ferrocene–estrogen conjugate. The hormone moiety is positioned in the estradiol binding pocket surrounded by the same hydrophobic core, the 17β-estradiol, but the position of the ferrocene varies among the conjugates. In the ferrocene conjugates **1**, **2b**, **4** and **5**, the hormone moieties adopt the same orientation as 17β-estradiol does. In **2a** and **3** the hormones are positioned in the LBP but opposite to the direction of 17β-estradiol. Thus, **2a** and **3** have the ferrocene groups positioned toward Arg394 and Glu353. **2b** gets engaged in hydrogen-bonding between the phenolic group (C(3)–OH) and Glu353, as 17β-estradiol does but in **3**; the hydrogen-bonding is between Glu353 and C(17)–O–H. The ferrocene group in **1**, **2a** and **3** resides in the subpocket cavity which connects with the main LBP through the Glu353 and Arg394 amino acid residues (extension from the 17β-estradiol LBP). This subpocket binding site is made of up to 55% of hydrophobic amino acid residues which include: Leu453, Trp360, Glu323, Pro324, Phe445, Lys449, Ile386, Trp393 and Gly390.

In terms of BA to the ERα ligand-binding pocket, **1** has the lowest value and is the most cytotoxic followed by **3**. Both are the most cytotoxic with the highest affinities. Based on these empirical results, we can envision that the cytotoxic activity of **1** is more correlated to the ERα recognition while for **3** it could be a combination of receptor recognition and the redox properties. For comparison, the BA of 17β-estradiol and ferrocene were calculated to be −12.5 kcal mol^{-1} and −5.7 kcal mol^{-1} respectively. Thus, the affinity of the ferrocene conjugates to the LBP is a combination of the estradiol and the hydrophobic contribution of the ferrocene. Lastly, with regard to **2a** and **2b** conformers, the position of the ferrocene group (α and β faces) makes significant differences in terms of the BA. In this regard, the beta conformer is energetically more favorable over the alpha conformer inside the LBP.

Cytotoxic studies

To gain insights into the structure–activity relationship, the cytotoxic activity of the ferrocene–hormone conjugates was determined in hormone-dependent MCF-7 and T-47D and hormone-independent MDA-MB-231 breast-cancer cell lines and compared to tamoxifen activity on the same cell lines as the standard. Tamoxifen is the gold standard drug to treat hormone-dependent breast cancer. In addition, tamoxifen is a selective estrogen receptor modulator (SERM) and a well-known established antiestrogen drug. Table 2 shows the IC_{50} values for the ferrocene–hormone conjugates on breast cancer cell lines.

Fc^+ being the species responsible for the genotoxic effect, we expect **3**, **4** and **5** to exhibit higher cytotoxic activities. However, the IC_{50} values of **3**, **4** and **5** cannot be correlated to their oxidation potentials. **1** is the most cytotoxic and has a higher *Epa* and the second most active conjugate, **3**, has an *Epa* lower than ferrocene. For **3** to have this cytotoxic activity (IC_{50} = 15(1), and 8(2) μM for MCF-7 and T-47D cell lines, respectively), the combination of ERα recognition combined with the facile oxidation of **3** could contribute to the total cytotoxic activity. On the other hand, the cytotoxic activities of **2**, **4**, and **5** are very similar in MCF-7 and T-47D cell lines while for the MDA-MD-231 cell line, **2** has substantially lower cytotoxic activity. Neither the redox potentials nor the binding affinity of these species can explain their behaviors and suggest that other targets can be involved in their mechanism of action. Nevertheless, the correlation between the redox potentials and the cytotoxic activities of the ferrocene conjugates must be taken into account with caution since the electrochemical experiments were performed in non-aqueous media. But it is necessary to emphasize the significant difference in the predicted binding affinity between **1** and the other ferrocene conjugates, suggesting that the cytotoxic activity of **1** could be more influenced by the ERα recognition, even though, it is the most robust to oxidize among the ferrocene conjugates.

The above results may be inconsistent when comparing the cytotoxic activities of compound **1** on the hormone-dependent and hormone-independent cell lines. In the MDA-MB-231 cell line, **1** has cytotoxic activity, although lower than in MCF-7. These results seem reasonable due to the fact that the estrogen receptor alpha protein is overexpressed in the MCF-7 cell line. However, **1** is more active on MDA-MB-231 than it is on the T-47D cancer cell line which is also hormone-dependent. In fact, the activity of compounds **4** and **5** through all the cell lines does not change significantly. To have an idea of the selectivity between the cell lines, we took the average of the activity of the compounds in the hormone-dependent cell lines and compared it with the activity of the hormone-independent cell line. Compounds **1**, **4**, and **5** show selectivity indexes of 1.06, 1.03, and 1.18, respectively. This result reflects that there is no apparent selectivity between the cell lines. However, compounds **2** and **3** showed a higher selectivity index in favour of the hormone-dependent cell lines, yielding selectivity indexes of 2.86 and 3.57, respectively. But when we compared our conjugates with the cytotoxic activity of tamoxifen, **1**, **3** and **4** are very similar in terms of the cytotoxic activity in the three cell lines studied, under the same experimental conditions. Table S2,† shows some of the previously cytotoxic studies of tamoxifen in the same cell lines used in this study. In none of the studies tamoxifen shows any apparent selectivity between the hormone-dependent MCF-7 and T-47D and hormone-independent MDA-MB-231 cell lines.[21–25]

Under this scenario, we cannot rule out the possibility of other proteins that may be targets for these ferrocene conjugates. The subject ferrocene conjugates have the ability to bind to the estrogen receptor beta protein (an isoform of the estrogen receptor alpha protein), as tamoxifen does. This receptor is present in the cell lines under study.[26,27] Moreover, the recent deorphanized membrane protein, a G-Protein Couple Receptor (GPER) binds estrogens and also plays an important

Table 2 Cytotoxicity of the ferrocene conjugates studied on hormone-dependent MCF-7 and T-47D, and hormone-independent MDA-MB-231 breast cancer cell lines as determined by the MTT assay after 72 h of drug exposure. IC_{50} values are based on quadruplicate experiments and standard deviation in parentheses

Ferrocene–hormone conjugates	MCF-7 (μM)	T-47D (μM)	MDA-MB-231 (μM)	Selectivity index[a]
1	9 (2)	23 (3)	17 (2)	1.06
2	45 (5)	27 (2)	103 (4)	2.86
3	15 (1)	8 (2)	41 (1)	3.57
4	32 (3)	34 (3)	34 (2)	1.03
5	22 (4)	27 (3)	29 (1)	1.18

[a] $\text{Selectivity index} = \dfrac{\text{Hormone independent } IC_{50} \text{ value}}{\text{Hormone dependent } IC_{50} \text{ values}} = \dfrac{MDA-MB-231\ IC_{50}}{(MCF-7\ IC_{50} + T-47D\ IC_{50})/2}$.

role in the estrogenic mechanisms of these cells. The latter is over-expressed in both MCF-7 and MDA-MB-231 breast cancer cell lines.[28] In fact, complexes **1**, **4** and **5** show similar cytotoxic activities on the MCF-7 and MDA-MB-231 breast cancer cell lines to some of the hydroxyferrocifen hybrids synthesized by Jaouen *et al.* on the same cell lines.[29]

At this point, based on the docking studies, it is difficult to attribute an anti-estrogenic effect to the subject ferrocene conjugates, at least as the main criteria, to justify their cytotoxic activities on the studied cancer cell lines. It is known that the anti-estrogenic power that some SERMs elicit, upon complexation to the estrogen receptor, is due to its ability to induce changes in the position of the helix12 (H12) of the estrogen receptor,[20] thus inhibiting the recruitment with coactivators that are responsible for the transcription factor once inside the cell nucleus. On the other hand, some synthetic agonists with a C-17 ethynyl linker between the estradiol and the europium and ferrocene conjugates[30,31] position the metal groups away from LBP, but H12 remains in the agonist conformation for coactivator recruitment. In particular for ferrocene–C(17)–estradiol conjugates, this strongly suggests that the agonist mechanism of the ER appears to overcome possible genotoxic damage from the ferrocene moiety. In this study none of the ferrocene conjugates showed the abovementioned binding interactions to the ERα-LBP. In fact, the available crystallographic structure of ERα in complexes with both agonist and antagonist ligands exhibits some structural and binding interaction features in common in the LBP that mimic endogenous ligands, such as the hydrogen-bonding network between the Glu353, Arg394 and the phenolic group of the ligand.[32] On the other hand, it cannot rule out the possibility of ligands with new forms of interaction with the estrogen receptor that could induce conformational changes inside the LBP such as disrupting binding-pocket key residue interactions (hydrogen-bonding, hydrophobic interactions), positioning them in a nonproductive conformation and destabilizing the H12 agonist conformation. The new conformation may lead to a series of physiological events in both genomic and non-genomic mechanisms, resulting in an anti-proliferative effect. This is a nonconventional mechanism proposed by Shiau *et al.* and these types of ligands are referred to as passive antagonists.[33]

As proposed by Shiau *et al.*,[33] the ligand-free ER LBD, in solution, is in equilibrium between inactive and active agonist-bound conformations. What a ligand does upon binding is shifting the equilibrium to a new position either agonist, antagonist or some conformation between these. But, at the present time, the docking of these conjugates inside the LBP only suggests the possibility of the selected estrogens to become vectors and be recognized by the receptor. Once inside the LBP, the ferrocene may or may not elicit its cytotoxic effect.

Materials and methods

Estrone and estradiol hormones, ferrocenecarboxaldehyde, Pd/C, 3-(4,5-dimethylthiazolyl-2)-2,5-diphenyltetrazolium bromide (MTT), silica gel (230–400 mesh), $CDCl_3$ and solvents were purchased from Sigma-Aldrich and used without further purification. ^{1}H NMR and ^{13}C NMR were performed using a Bruker 500 MHz Advance Bruker spectrometer. Shifts (δ) are given in parts per million (ppm) using the resonance of the solvent peak as a secondary reference ($\delta(^1H)$ = 7.26 pm and $\delta(^{13}C)$ = 77.16 ppm), for $CDCl_3$. Multiplicities are reported using the following abbreviations: s (singlet), d (doublet), t (triplet), q (quartet), m (multiplet). IR studies were performed using a FT-IR spectrometer Spectrum Two by PerkinElmer in the solid state. Crystals suitable for X-ray crystallography were directly obtained from the vapor diffusion technique. Intensity data were collected with a Bruker Kappa-APEXII Ultra using Mo-Kα radiation (λ = 0.71073 Å). Data collection was performed with the APEX2 suite (Bruker). Unit-cell parameter refinement, integration and data reduction were carried out with the SAINT program (Bruker). SADABS (Bruker) was used for scaling[34] and multi-scan absorption corrections and structure refinement by full-matrix least-squares methods using SHELXL-14.[35,36] Elemental analyses were performed by Atlantic Microlab, Georgia. The pure crystalline compounds are obtained as solvates, incorporating the crystallizing or reaction solvent ($CHCl_3$ or H_2O) into the unit cell as will be evident in the X-ray diffraction studies.

Experimental

Docking studies

Protein-drug docking studies were performed using the AutoDock Vina[37] program in order to evaluate the conformation and the relative score of energy affinity provided by the program, which represents the predicted binding energy (BA) among the ferrocene complexes into the ERα-LBD in terms of *in silico* protein–ligand interaction. Analysis of the binding site was performed employing the Pocket Volume Measure (POVME 2.0)[38] Algorithm to obtain a detailed picture of the important insights of protein–ligand recognition. The PDB file of the ERα-LBD protein of interest was obtained from The Research Collaborator for Structural Bioinformatics Protein Data Bank (RCSB PDB),[39] while the ferrocene conjugate structures were obtained from the single crystal X-ray diffraction, as previously described. NMR peak assignments follow the numbering of the X-ray structures.

The estrogen receptor alpha ligand binding domain

The monomeric structure (code: 2YAT) of the ERα-LBD-E2-Eu[4] complex was selected for the study.[30] The E2-Eu complex inside the LBD, water, metals, and any molecule that was not a fundamental part of the study were removed. A reconstruction of missed atoms was performed on some amino acid side-chains of the protein crystal structure using modeller 9.18.[40–42] Polar hydrogen and Gasteiger charge were computed and added to the protein structure and converted to pdbqt format using AutoDockTools (ADT)[43] software. Residues inside the LBD that surround the E2 molecule were selected to be either

flexible, or rigid. The grid box was located at the center of the E2 position into the ERα-LBD. Docking studies were performed in both ways: with and without the crystallographic water in the ERα-LBD structure to obtain a more detailed view of the role played by water on the ligand–protein binding energy by AutoDock Vina. The best poses and their predicted binding energy, BA, of each calculation were selected for the study. The initial coordinates of each one of the ferrocene complexes used for the docking studies were selected from the crystallographic data obtained. With the exception of **5**, all the crystallographic coordinates were within the expected bond distances and angles found in the literature as discussed previously. For the solid-state structure of **5** which contains 6 independent molecules in the unit cell, we came to realize the remarkable differences in some of their C16–C19–C20 bond angles. For example, conformer **5C** has a C16–C19–C20 bond angle of 97.01°, whereas for conformer **5A** it is 119.70° for the same angle. These angles are far away different for an idealized C19 sp^3 hybridization (109.5°). Due to the fact that Auto dock Vina only allows selected rotational bonds on ligands for docking analysis, choosing incorrect crystallographic coordinate residues could result in an overestimation of the docking ranking result. Thus, conformer **5F** was selected for the docking studies since the C16–C19–C20 angle is 110.20°, close to the sp^3 hybridization angle.

Cytotoxic studies on the breast-cancer cell line

The cytotoxicities of the ferrocene conjugates were determined by the MTT (3-(4,5-dimethylthiazol-2-yl)-2,5-diphenyltetrazolium bromide) colorimetric assay.[44,45] Viable cells with active metabolism convert MTT into a purple-colored formazan product by enzymatic action in the mitochondria, with absorbance near 570 nm. However, dead cells will not metabolize MTT to the formazan product. Therefore, the absorbance recorded at 570 nm is a direct correlation with the number of live cells in the assay.

Hormone-dependent MCF-7 and T-47D, and hormone-independent MDA-MB-231 breast-cancer cell lines were seeded into 96 well plates at 1×10^4 cells per well previously grown and incubated in their respective media according to American Type Culture Collection (ATCC) protocols. The cells seeded into the 96 well plates were incubated for a period of 24 hours in order to ensure cell adhesion in the plate, followed by addition of ferrocene drugs in a range of concentrations. The higher ferrocene conjugate concentration used was 0.01 M. After 72 hours of incubation, MTT solution was added at concentrations at 1 mg mL^{-1} per well and was incubated for two additional hours. After two hours, a solution of 2-propanol with Triton at 10% was added. A purple solution appears instantaneously as a result of the number of live cells. The half-maximal inhibitory concentration (IC_{50}) was calculated using a cell control without any drug.

Synthesis

3-Estradiol ferrocenecarboxylate (1). Fluorocarbonylferrocene was synthesized as previously described and used directly after column chromatography purification. To a solution of 46.6 mg (0.2 mmol) of fluorocarbonylferrocene and 36.7 mg, (0.3 mmol) of 4-dimethylaminopyridine in 2 mL dry CH_2Cl_2, 81.7 mg (0.3 mmol) of β-estradiol was added. The mixture was stirred and heated to reflux for 12 h. After reaction completion 2 mL of H_2O was added. The resulting orange-red organic layer was separated, and the aqueous phase was extracted with CH_2Cl_2 three times. The organic phase was dried over $CaCl_2$, gravity filtered and solvent evaporated under reduced pressure resulting in a red-orange amorphous solid. Purification by column chromatography using CH_2Cl_2 : ethyl acetate (7 : 3) as the mobile phase followed by solvent evaporation afforded a red-orange amorphous solid (85% yield). Red-orange single crystals suitable for X-ray diffraction crystallography were obtained after the vapor diffusion technique using $CHCl_3$: pentane. ATR-IR (cm^{-1}): 3512, 3111, 2940, 2917, 2868, 2051, 1985, 1886, 1719, 1493, 1453, 1106, 1090, 1016, 917, 821, 802, 764. ^{1}H NMR ($CDCl_3$): δ (ppm): 7.32 (H_2, d, 1H, J = 8.3 Hz), 6.94 (H_1, d, 1H, J = 8.1 Hz), 6.89 (H_3, s, 1H), 4.95 (H_{21}, H_{22}, s, 2H), 4.48 (H_{23}, H_{24}, s, 2H), 4.29 (H_{25-29}, s, 5H), 3.73 (H_{17}, s, 1H), 2.90 ($H_{6\alpha,\beta}$, s, 2H), 2.35 ($H_{11\alpha}$, d, 1H, J = 11.2 Hz), 2.24 ($H_{7\alpha}$, t, 1H, J = 9.9 Hz), 2.12 (H_9, m, 1H), 1.97 ($H_{16\alpha}$, d, 1H, J = 12.3 Hz), 1.90 ($H_{12\beta}$, d, 1H, J = 9.7 Hz), 1.71 ($H_{7\beta}$, m, 1H), 1.52–1.27 ($H_{15\alpha}$, $H_{16\beta}$, $H_{11\beta}$, H_8, $H_{15\beta}$, $H_{12\alpha}$, H_{14}, –O(2)H, m, 8H), 0.78 (H_{18}(–CH_3), s, 3H). ^{13}C NMR ($CDCl_3$): δ (ppm): (C═O) 170.51, (C_3) 148.54, (C_5, C_{10}) 138.18, (C_1) 137.70, (C_4) 126.36, (C_2) 121.58, (C_{20}) 118.68, (C_{17}) 81.82, 71.83, 70.60, 70.21, 69.92, 50.02, 44.13, 43.18, 38.48, 36.64, 30.53, 29.60, 27.05, 26.16, 23.11, 11.04. Anal. calc. for $C_{29}H_{32}O_3Fe$: C, 71.89; H, 6.67. Found: C, 71.92; H, 6.59.

16-Ferrocenylidene-3-hydroxyestra-1,3,5(10)-triene-17-one (2). To a stirred solution of 135.2 mg (0.5 mmol) of estrone in 5.6 mL of EtOH were added 117.7 mg (0.55 mmol) of ferrocenecarboxaldehyde and 10% KOH ethanolic solution (2.0 mL). The resulting red mixture was stirred for 4 h at r.t., and then neutralized with acetic acid. H_2O was added to precipitate the product. A red amorphous solid was obtained after filtration. Purification by column chromatography using CH_2Cl_2 : ethyl acetate (9 : 1) as the mobile phase, followed by solvent evaporation under reduced pressure afforded a red amorphous solid (86% yield).

Red crystals suitable for single crystal X-ray diffraction crystallography of **2a** and **2b** were obtained after slow evaporation employing benzene as the solvent and the liquid–liquid diffusion technique using hexane (**2a**) and in a mixture of $CHCl_3$: CCl_4 (**2b**). ATR-IR (cm^{-1}): 3337, 3090, 2963, 2920, 2859, 1979, 1693, 1604, 1502, 1444, 1224, 1103, 820, 720. ^{1}H NMR ($CDCl_3$): δ (ppm): 7.34 (H_{19}, s, 1H), 7.18 (H_2, d, 1H, J = 8.4 Hz), 6.68 (H_1, dd, 1H, J = 8.4, 2.6), 6.62 (H_3, d, 1H, J = 2.5), 5.16 (–OH, s, 1H), 4.56 (H_{21}, H_{22}, dt, 2H, J = 11.41, 1 Hz), 4.44 (H_{23}, H_{24}, dd, 2H, J = 17.3, 1 Hz), 4.14 (H_{25-29}, s, 5H), 2.92 ($H_{6\alpha,\beta}$, m, 2H), 2.80 ($H_{11\alpha}$, ddd, 1H, J = 15.3, 6.45, 1.3 Hz), 2.42 ($H_{7\alpha}$, m, 1H), 2.30 (H_9, m, 1H), 2.22 ($H_{12\beta}$, m, 1H), 2.07 ($H_{7\beta}$, $H_{15\beta}$, m, 2H), 1.60 ($H_{15\alpha}$, H_{14}, $H_{12\alpha}$, $H_{11\beta}$, H_8, m, 5H), 0.97 (H_{18}(–CH_3), s, 3H). ^{13}C NMR ($CDCl_3$); δ (ppm): (C═O)209.51, (C_3)153.62, (C_5) 137.95, (C_{10})134.69, (C_1)132.26, (C_4)132.08, (C_2)126.48, (C_{16})

115.30, (C_{19})112.87, 78.77, 71.66, 70.96, 69.55, 48.31, 47.87, 44.03, 37.90, 31.60, 29.49, 28.52, 26.80, 25.99, 14.78. Anal. calc. for $C_{29}H_{30}O_2Fe{\cdot}0.25CHCl_3$ (contains 0.25 mol of $CHCl_3$): C, 70.80; H, 6.14. Found: C, 71.13; H, 6.18.

16-Ferrocenylidene-17β-estra-1,3,5-triene-3,17-diol (3). To a solution of **2** (55.94 mg, 0.12 mmol) in EtOH (3.25 mL) at 0 °C was added 7.6 mg (0.2 mmol) of $NaBH_4$ for 3–4 h at 0 °C. The reaction was quenched by the addition of H_2O. To decompose the borate ether, 0.75 mL of 3 M NaOH solution was added to the reaction. The aqueous phase was extracted with ethyl acetate three times. The organic phase was dried over $CaCl_2$, gravity filtered and solvent evaporation under vacuum yields an orange-yellow amorphous solid. Purification by column chromatography using CH_2Cl_2 : ethyl acetate (9 : 1) as the mobile phase and solvent evaporation under reduced pressure afforded an orange-yellow amorphous solid (99% yield). Orange single crystals were obtained after the vapor diffusion technique using $CHCl_3$: pentane. ATR-IR (cm^{-1}): 3431, 3240, 3097, 2959, 2925, 2905, 2827, 1982, 1770, 1609, 1601, 1504, 1450, 1379, 1140, 1047, 815, 812. ^{1}H NMR ($CDCl_3$): δ (ppm): 7.18 (H_2, d, 1H, J = 9.4 Hz), 6.65 (H_1, dd, 1H, J = 8.6, 2.7 Hz), 6.59 (H_3, d, 1H, J = 1 Hz), 6.23 (H_{19}, d, 1H, J = 2.2 Hz), 4.72 (–O(1)H, s, 1H), 4.38 (H_{21}, H_{22}, dd, 2H, J = 13.2, 1.4 Hz), 4.21 (H_{23}, H_{24}, t, 2H, J = 1 Hz), 4.07 (H_{25-29}, s,d, 5H), 2.88 ($H_{6\alpha,\beta}$, m, 2H), 2.57 ($H_{11\alpha}$, dd, 1H, J = 16.5, 6.6 Hz), 2.37 ($H_{7\alpha}$, m, 1H), 2.29 (H_9, td, 1H, J = 10.6, 3.7 Hz), 2.03 ($H_{7\beta}$, $H_{15\beta}$, $H_{12\beta}$, m, 3H), 1.60 (–O(2)H s, 1H), 1.41 (H_{17}, $H_{15\alpha}$, H_{14}, $H_{12\alpha}$, $H_{11\beta}$, H_8, m, 6H), 0.70 (H_{18}(–CH_3), s, 3H). ^{13}C NMR ($CDCl_3$): δ (ppm): (C_3)153.36, (C_{16})142.09, (C_5)138.16, (C_{10})132.56, (C_1)126.51, (C_{19})119.96, (C_4)115.26, (C_2)112.72, (C_{20})84.78, (C_{17})82.72, 68.96, 68.53, 68.38, 47.26, 44.03, 43.20, 38.29, 36.26, 30.24, 29.57, 27.39, 26.33, 11.05. Anal. calc. for $C_{29}H_{32}O_2Fe{\cdot}0.5H_2O$ (contains 0.5 mol of H_2O): C, 72.96; H, 6.97. Found: C, 73.01; H, 6.92.

16-Ferrocenemethyl-3β-hydroxyestra-1,3,5(10)-triene-17-one (4). To a solution of 56.2 mg (0.12 mmol) of **2** in 1.2 mL of EtOH : THF (1 : 1) was added 5.6 mg of palladium on charcoal (10% weight) under a hydrogen atmosphere and stirred at r.t. for 12 h. The palladium reagent was removed by filtration on Celite, washed with EtOH and solvent evaporated under vacuum affording a yellow amorphous solid. Purification by column chromatography using CH_2Cl_2 : ethyl acetate (9 : 1) as the mobile phase and solvent evaporation under reduced pressure afforded compounds **4** and **5** as yellow amorphous solids (54% and 43% yield respectively). Yellow plate crystals of **4** were obtained after slow evaporation using the $CHCl_3$ solvent. ATR-IR (cm^{-1}): 3354, 3088, 2921, 2868, 1982, 1890, 1719, 1607, 1502, 1448, 1286, 1225, 1104, 914, 874, 821, 663. ^{1}H NMR ($CDCl_3$): δ (ppm): 7.13 (H_2, s, 1H), 6.63 (H_1, dd, 1H, J = 8.4, 2.7 Hz), 6.57 (H_3, d, 1H, J = 2.6 Hz), 4.72 (–OH, d, 1H, J = 4.3 Hz), 4.11–4.04 (H_{21-29}, s, m, m, m 9H), 2.89 ($H_{6\alpha,\beta}$, dd, 1H, J = 8.9, 4.0 Hz), 2.83 ($H_{11\alpha}$, m, 2H), 2.54 ($H_{7\alpha}$, dd, 1H, J = 14.2, 8.9 Hz), 2.28 (H_9, $H_{12\beta}$, H_{19}, m, 3H), 2.06 ($H_{16\alpha}$, m, 1H), 1.95 ($H_{7\beta}$, $H_{15\beta}$, m, 2H), 1.41 ($H_{15\alpha}$, H_{14}, $H_{12\alpha}$, $H_{11\beta}$, H_8, H_{19}, m, 6H), 0.66 (H_{18}(–CH_3), s, 3H). ^{13}C NMR ($CDCl_3$): δ (ppm): (C_3)153.43, (C_5)138.05, (C_1)132.13, (C_2)126.47, (C_{10})115.25, 112.76, (C_{20}) 86.15, 69.49, 68.61, 67.59, 67.48, 51.79, 48.88, 48.46, 44.07, 37.73, 31.92, 31.71, 29.45, 27.95, 26.66, 25.85, 13.60. Anal. calc. for $C_{29}H_{32}O_2Fe{\cdot}0.5H_2O$ (contains 0.5 mol of H_2O): C, 72.96; H, 6.97. Found: C, 72.91; H, 6.97.

16-Ferrocenemethyl-17β-estra-1,3,5(10)-triene-3,117-diol (5). Ferrocene conjugate **5** was obtained either employing **2** or **3** as the starting material under the already described experimental conditions of **4**. Compound **5** was obtained as a single product when **3** was used as the starting material. Yellow plate crystals were obtained after slow evaporation using the $CHCl_3$: EtOH solvent. ATR-IR (cm^{-1}): 3530, 3351, 3097, 2977, 2923, 2866, 1981, 1867, 1613, 1603, 1500, 1450, 1450, 1285, 1451, 1104, 1000, 815. ^{1}H NMR ($CDCl_3$): δ (ppm): 7.15 (H_2, d, 1H, J = 8.4 Hz), 6.62 (H_1, d, 1H, J = 8.4 Hz), 6.55 (H_3, d, 1H, J = 2.4 Hz), 4.57 (–O(1)H, s, 1H), 4.11–4.06 (H_{21-29}, m, dd, 9H), 2.79 ($H_{6\alpha,\beta}$, m, 2H), 2.54 ($H_{11\alpha}$, qd, 1H), 2.23 (H_9, $H_{12\beta}$, $H_{7\alpha}$, m, 3H), 2.05 ($H_{16\alpha}$, s, 1H), 1.89 ($H_{7\beta}$, H_{19}, $H_{12\beta}$, m, 3H), 1.54 ($H_{15\beta}$, –O(2)H, H_{14}, m, 3H), 1.31 ($H_{7\beta}$, $H_{12\alpha}$, H_{19}, $H_{11\beta}$, H_8, m, 5H), 1.07 ($H_{15\alpha}$, m, 1H), 0.79 (H_{18}(–CH_3), 2s, 3H). ^{13}C NMR (CDCl3): δ (ppm): (C_3)153.25, (C_5)138.29, (C_{10})132.77, (C_1)126.52, (C_4)115.20, (C_2) 112.62, (C_{20})87.61, (C_{17})82.29, 68.64, 48.48, 48.24, 46.09, 44.27, 43.99, 42.48, 38.44, 38.19, 37.66, 36.82, 35.75, 32.69, 31.78, 30.39, 29.58, 27.35, 27.17, 26.25, 12.55, 11.92. Anal. calc. for $C_{29}H_{32}O_2Fe{\cdot}0.5H_2O$ (contains 0.5 mol of H_2O): C, 72.96; H, 6.97. Found: C, 72.54; H, 7.17.

Conclusion

The development of novel organometallic drugs is a growing area of interest that requires fundamental research of the organometallic complex, development of its synthetic methodology and its application to biological systems. All the functionalized ferrocene–hormone conjugates presented in this work have been characterized successfully, for the first time, by the X-ray diffraction technique in order to determine their structures and spatial arrangements as an important aspect to understand their mode of action and interaction with biological systems. This is a prerequisite for the development of new drugs. Some of the intrinsic properties of these conjugates have been delineated using as the spearhead the information obtained from the solid state and its connection with the cytotoxic activity on the hormone-dependent and -independent breast-cancer cell lines. The data suggest that the estrogens in the ferrocene conjugates (at position 3 or 16) could serve as vectors and be recognized by ERα as a delivery mechanism into the cell.

The incorporation of the ferrocene group into the principal estrogen skeleton represents a remarkable structure volume addition. Despite the common chemical properties that ferrocene and benzene have, aromaticity criteria and synthetic homology, ferrocene bulkiness is nearly 60% more than benzene (130.4 Å^3 *vs.* 77.1 Å^3). This structural difference could result in steric hindrance upon complexation with the receptor. This has been a common strategy employed in the literature, where aromatic groups are substituted by ferrocene, by the only presumption of its common aromaticity criteria on

natural or synthetic biologically active compounds. However, the rational incorporation of the ferrocene group could result in great advantages in the process of drug design if its spatial distribution along with its intermolecular forces are congruent with the cavity of protein binding sites. This approach could result in an enhancement in the cytotoxic activity of ferrocene conjugates due to a synergistic effect by combining the protein recognition and the intrinsic ferrocene ROS production activity. Our ongoing efforts are aimed at improving some of the structural features of the vectors that are necessary to mimic key interactions found in natural and synthetic ligands of the ER, based on the strength of individual bonding interactions and their contribution to the overall free-energy of complexation.

X-ray crystallography

The CIF files for the crystal structures of **1**, **2a**, **2b**, **3**, **4** and **5** have been deposited in the CCDC and have been given the deposition numbers 1842145, 1842142, 1842144, 1842143, 1842141, 1842140 respectively.†

Conflicts of interest

There are no conflicts to declare.

Acknowledgements

José A. Carmona-Negrón and Enrique Meléndez acknowledge the financial support from the BioXFEL Science Technology Center (STC A.N 1231306), the NSF-CREST II 000743-00002, the Alfred P. Sloan Program, the American Society of Biochemistry and Molecular Biology, and the American Crystallography Association (ACA). Special thanks to Dr Roberto Rios for allowing us to perform the catalytic hydrogenation in his laboratory, Dr Oscar Morales for helping to complete ferrocene conjugate spectroscopic data due to Hurricane Maria's damage on our Department of Chemistry, Dr Wanda I. Pérez for MTT protocol assistance and Ms Mariola M. Flores-Rivera for their time dedicated to assist in the synthesis and purification of ferrocene derivatives, and Dr Carmen Ortiz and Dr Jaime Matta for their generosity of providing the MDA-MB-231 breast cancer cell line to our laboratory. We also acknowledge the assistance of Dr Luis Morell for proofreading this manuscript.

Notes and references

1 S. Dasari and P. Bernard Tchounwou, *Eur. J. Pharmacol.*, 2014, **740**, 364–378.
2 J. Guan, Y. Zhang, Q. Li, Y. Zhang, L. Li, M. Chen, N. Xiao, L. Chen, J. Guan, Y. Zhang, Q. Li, Y. Zhang, L. Li, M. Chen, N. Xiao and L. Chen, *Oncotarget*, 2016, **7**, 70185–70193.
3 Z. H. Siddik, *Oncogene*, 2002, **22**, 7265.
4 K. Barabas, R. Milner, D. Lurie and C. Adin, *Vet. Comp. Oncol.*, 2008, **6**, 1–18.
5 O. Kanat, H. Ertas and B. Caner, *World J. Clin. Oncol.*, 2017, **8**, 329–335.
6 X. Yao, K. Panichpisal, N. Kurtzman and K. Nugent, *Am. J. Med. Sci.*, 2007, **334**, 115–124.
7 K. Woźniak and J. Błasiak, *Acta Biochim. Pol.*, 2002, **49**, 583–596.
8 P. Köpf-Maier, H. Köpf and E. W. Neuse, *J. Cancer Res. Clin. Oncol.*, 1984, **108**, 336–340.
9 G. Gasser, I. Ott and N. Metzler-Nolte, *J. Med. Chem.*, 2011, **54**, 3–25.
10 B. Albada and N. Metzler-Nolte, *Acc. Chem. Res.*, 2017, **50**, 2510–2518.
11 B. Albada and N. Metzler-Nolte, *Chem. Rev.*, 2016, **116**, 11797–11839.
12 M. Patra and G. Gasser, *Nat. Rev. Chem.*, 2017, **1**, 0066.
13 G. Tabbì, C. Cassino, G. Cavigiolio, D. Colangelo, A. Ghiglia, I. Viano and D. Osella, *J. Med. Chem.*, 2002, **45**, 5786–5796.
14 D. Osella, H. Mahboobi, D. Colangelo, G. Cavigiolio, A. Vessières and G. Jaouen, *Inorg. Chim. Acta*, 2005, **358**, 1993–1998.
15 H. Tamura and M. Miwa, *Chem. Lett.*, 1997, **26**, 1177–1178.
16 X. Narváez-Pita, A. L. Rheingold and E. Meléndez, *J. Organomet. Chem.*, 2017, **846**, 113–120.
17 J. A. Carmona-Negrón, M. M. Flores-Rivera, Z. Díaz-Reyes, C. E. Moore, A. L. Rheigold and E. Meléndez, *Acta Crystallogr., Sect. E: Crystallogr. Commun.*, 2016, **72**, 868–871.
18 S. Top, B. Dauer, J. Vaissermann and G. Jaouen, *J. Organomet. Chem.*, 1997, **541**, 355–361.
19 J. Vera, L. M. Gao, A. Santana, J. Matta and E. Meléndez, *Dalton Trans.*, 2011, **40**, 9557–9565.
20 A. M. Brzozowski, A. C. Pike, Z. Dauter, R. E. Hubbard, T. Bonn, O. Engström, L. Ohman, G. L. Greene, J. A. Gustafsson and M. Carlquist, *Nature*, 1997, **389**, 753–758.
21 H. Seeger, J. Huober, D. Wallwiener and A. O. Mueck, *Horm. Metab. Res.*, 2004, **36**, 277–280.
22 N. Abu, M. Akhtar, W. Ho, S. Yeap, N. Alitheen, N. Abu, M. N. Akhtar, W. Y. Ho, S. K. Yeap and N. B. Alitheen, *Molecules*, 2013, **18**, 10367–10377.
23 S. Weng, Y. Kashida, S. K. Kulp, D. Wang, R. W. Brueggemeier, C. L. Shapiro and C. Chen, *Mol. Cancer Ther.*, 2008, **7**, 800–808.
24 N. Abu, M. N. Akhtar, S. K. Yeap, K. L. Lim, W. Y. Ho, A. J. Zulfadli, A. R. Omar, M. R. Sulaiman, M. P. Abdullah and N. B. Alitheen, *PLoS One*, 2014, **9**, e105244.
25 S. Rajput, B. N. P. Kumar, S. Sarkar, S. Das, B. Azab, P. K. Santhekadur, S. K. Das, L. Emdad, D. Sarkar, P. B. Fisher and M. Mandal, *PLoS One*, 2013, **8**, e61342.
26 M. D. Al-Bader, C. Ford, B. Al-Ayadhy and I. M. Francis, *Exp. Ther. Med.*, 2011, **2**, 537–544.
27 E. A. Vladusic, A. E. Hornby, F. K. Guerra-Vladusic, J. Lakins and R. Lupu, *Oncol. Rep.*, 2000, **7**, 157–224.

28 C. M. Revankar, D. F. Cimino, L. A. Sklar, J. B. Arterburn and E. R. Prossnitz, *Science*, 2005, **307**, 1625–1630.
29 J. de J. Cázares-Marinero, S. Top, A. Vessières and G. Jaouen, *Dalton Trans.*, 2013, **43**, 817–830.
30 M.-J. Li, H. M. Greenblatt, O. Dym, S. Albeck, A. Pais, C. Gunanathan, D. Milstein, H. Degani and J. L. Sussman, *J. Med. Chem.*, 2011, **54**, 3575–3580.
31 A. Vessières, D. Spera, S. Top, B. Misterkiewicz, J.-M. Heldt, E. Hillard, M. Huché, M.-A. Plamont, E. Napolitano, R. Fiaschi and G. Jaouen, *ChemMedChem*, 2006, **1**, 1275–1281.
32 A. C. W. Pike, *Best Pract. Res., Clin. Endocrinol. Metab.*, 2006, **20**, 1–14.
33 A. K. Shiau, D. Barstad, J. T. Radek, M. J. Meyers, K. W. Nettles, B. S. Katzenellenbogen, J. A. Katzenellenbogen, D. A. Agard and G. L. Greene, *Nat. Struct. Biol.*, 2002, **9**, 359–364.
34 *APEX2, SAINT and SADABS*, Bruker AXS, Inc., Madison, Wisconsin, USA, 2013.
35 G. M. Sheldrick, *Acta Crystallogr., Sect. A: Found. Adv.*, 2015, **71**, 3–8.
36 G. M. Sheldrick, *Acta Crystallogr., Sect. C: Struct. Chem.*, 2015, **71**, 3–8.
37 O. Trott and A. J. Olson, *J. Comput. Chem.*, 2010, **31**, 455–461.
38 J. D. Durrant, L. Votapka, J. Sørensen and R. E. Amaro, *J. Chem. Theory Comput.*, 2014, **10**, 5047–5056.
39 H. M. Berman, J. Westbrook, Z. Feng, G. Gilliland, T. N. Bhat, H. Weissig, I. N. Shindyalov and P. E. Bourne, *Nucleic Acids Res.*, 2000, **28**, 235–242.
40 N. Eswar, B. Webb, M. A. Marti-Renom, M. S. Madhusudhan, D. Eramian, M. Shen, U. Pieper and A. Sali, *Curr. Protoc. Bioinf.*, 2006, **15**, 5.6.1–5.6.30.
41 A. Šali and T. L. Blundell, *J. Mol. Biol.*, 1993, **234**, 779–815.
42 A. Fiser, R. K. G. Do and A. Šali, *Protein Sci.*, 2000, **9**, 1753–1773.
43 G. M. Morris, R. Huey, W. Lindstrom, M. F. Sanner, R. K. Belew, D. S. Goodsell and A. J. Olson, *J. Comput. Chem.*, 2009, **30**, 2785–2791.
44 F. Denizot and R. Lang, *J. Immunol. Methods*, 1986, **89**, 271–277.
45 T. Mosmann, *J. Immunol. Methods*, 1983, **65**, 55–63.